

Pd/PdO Electrocatalysts Boost Their Intrinsic Nitrogen Reduction Reaction Activity and Selectivity *via* Controllably Modulating the Oxygen Level

Qianqian Chen, Xuemei Zhou,* Xiaodong Zhang, Wenjie Luo, Shuo Yang, Yongjie Ge, Dong Cai, Huagui Nie,* and Zhi Yang*



Cite This: *ACS Appl. Mater. Interfaces* 2022, 14, 20988–20996



Read Online

ACCESS |



Metrics & More



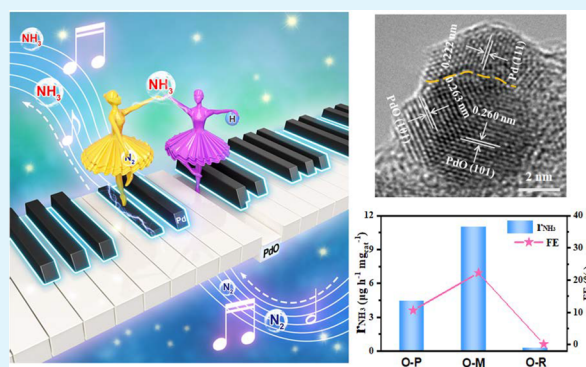
Article Recommendations



Supporting Information

ABSTRACT: The electrocatalytic nitrogen reduction reaction (eNRR) is regarded as promising sustainable ammonia (NH_3) production alternative to the industrial Haber–Bosch process. However, the current electrocatalytic systems still exhibit a grand challenge to simultaneously boost their eNRR activity and selectivity under ambient conditions. Herein, we construct Pd/PdO electrocatalysts with a controlled oxygen level by a facile electrochemical deposition approach at different gas atmospheres. Theoretical calculation results indicate that the introduction of an oxygen atom into a pure Pd catalyst would modulate the electron density of the Pd/PdO heterojunction and thus influence the adsorption energy for nitrogen and hydrogen. The calculation results and experiments show that the Pd/PdO heterojunction with a moderate oxygen level (O-M) exhibits optimal eNRR performance with a high NH_3 yield of $11.0 \mu\text{g h}^{-1} \text{mg}_{\text{cat}}^{-1}$ and a large Faraday efficiency (FE) of 22.2% at 0.03 V (vs RHE) in a 0.1 M KOH electrolyte. The moderate affinity of Pd to N in the Pd/PdO heterojunction and the inhibition of the hydrogen evolution reaction (HER) can facilitate the breaking of the triple bond of N_2 and promote the protonation of N, which is confirmed by *ex situ* X-ray photoelectron spectroscopy (XPS) and *in situ* Raman spectroscopy. *In situ* Fourier transform infrared spectroscopy (FTIR) and density functional theory (DFT) calculations further disclose that the O-M catalysts prefer the distal association pathway during the eNRR process. This work opens a new way to construct heterostructures by controlling the oxygen level in other electrochemical fields.

KEYWORDS: Pd/PdO heterojunction, electrocatalyst, nitrogen reduction reaction, controllable modulation, oxygen level



1. INTRODUCTION

The electrocatalytic nitrogen reduction reaction (eNRR) is a green and environmentally friendly approach that synthesizes ammonia (NH_3) from air and water with renewable electricity at ambient temperature and pressure.^{1–5} Hence, the eNRR is considered a promising sustainable alternative to the industrial Haber–Bosch process.^{6–10} Despite the considerable advances, the electrocatalysts still cannot simultaneously produce high selectivity and activity for the eNRR. In view of the poor N_2 adsorption and high activation barrier for splitting N–N triple bonds, the developed electrocatalysts exhibit a higher overpotential for the eNRR than for the hydrogen evolution reaction (HER), thus resulting in the limited selectivity and activity for the eNRR in aqueous solutions.

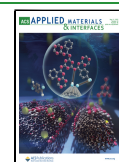
To solve the dilemma, various strategies have been constructed in the past few years. A facile method is to use aqueous electrolytes with different pH or additives (*e.g.*, Li^+ ,¹¹ K^+ ,^{12,13} polyethylene glycol¹⁴) to suppress the HER by limiting the proton concentration on the catalyst surfaces.¹⁵ However,

too few protons do not initiate the proton-coupled electron-involved eNRR. Apart from varying the electrolyte solutions, single metals with different structures can also function as mediators for the dilemma of selectivity and activity in the eNRR.^{16,17} Theoretical calculation and experimental results suggest that single metals with a higher nitrogen adsorption ability than hydrogen exhibit a higher eNRR selectivity.^{7,16,18–20} However, too strong a binding to nitrogen species would be unfavorable for the subsequent desorption of certain intermediates during the eNRR, which results in poisoning of the metal catalysts. To mitigate the limitations by the scaling relations and efficiently enhance the intrinsic eNRR activity,

Received: February 7, 2022

Accepted: April 13, 2022

Published: April 29, 2022



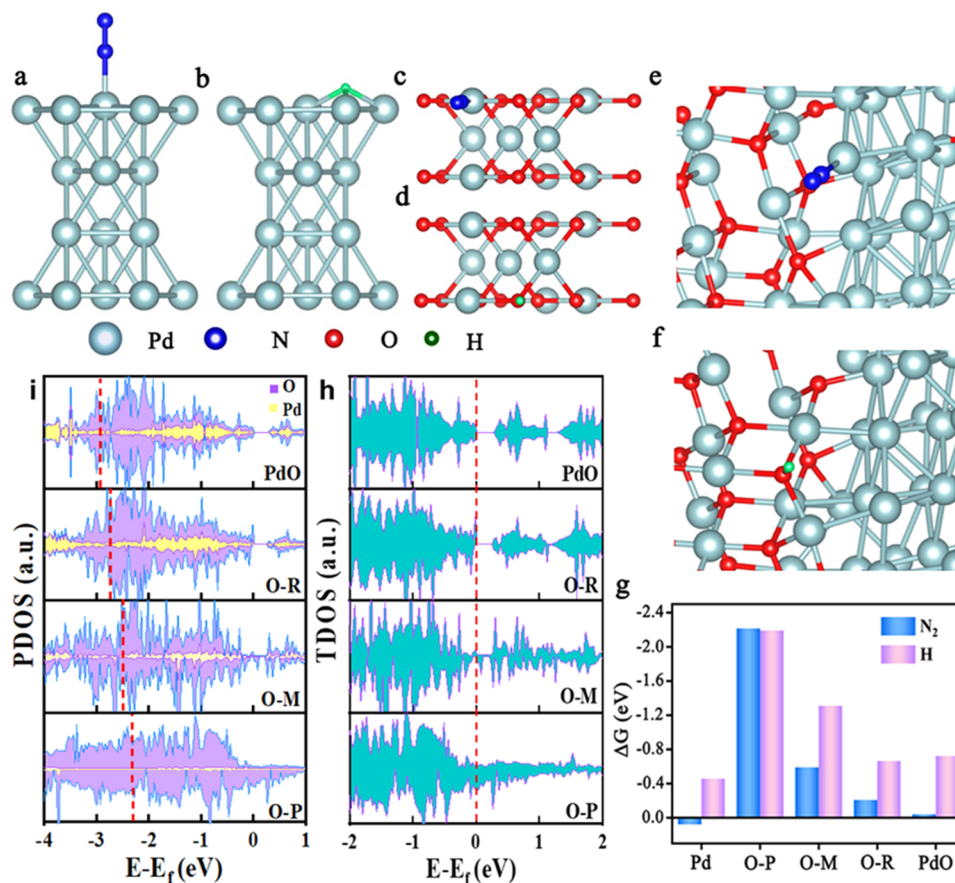


Figure 1. Optimum adsorption sites of Pd (a, b), PdO (c, d), and the O-M Pd/PdO catalyst (e, f) for N₂ and H, respectively. The Pd, N, O, and H atoms are presented by silvery gray, blue, red, and green solid balls, respectively. (g) Optimal adsorbed energies of five models catalysts for N₂ and H. TDOS (h) and (i) PDOS of O-P, O-M, O-R, and PdO catalysts, respectively.

several groups have resorted to alloy or metal/semiconductor catalysts to tune their electron density.^{21,22} The produced appropriate electron density could efficiently regulate the adsorption of the catalysts toward nitrogen against hydrogen in aqueous electrolytes, thus elevating the eNRR activity and simultaneously depressing the HER. Although advances have been achieved, these electrocatalysts exhibit limited eNRR performances. Hence, rational exploration of more efficient electrocatalysts is still a great opportunity to promote the thermodynamics and kinetics for the eNRR in aqueous electrolytes at a low overpotential.

Recently, several groups found that metal/metal oxide catalysts may show higher activity for the eNRR.^{22–24} There is a certain understanding of the eNRR mechanism of these catalysts; however, it still needs to be deeply investigated. Herein, we construct a Pd/PdO heterostructure *via* controllably modulating the oxygen level to boost the intrinsic eNRR activity and selectivity of Pd-based catalysts. Combining density functional theory (DFT) calculation and experiments, we find that oxygen-moderate (O-M) Pd/PdO heterostructures with an appropriate nitrogen-species-adsorption energy show higher NH₃ yields and Faraday efficiencies (FEs) compared with those of oxygen-poor (O-P) and oxygen-rich (O-R) Pd/PdO catalysts. *Ex situ* (X-ray photoelectron spectroscopy (XPS)) and *in situ* spectroscopic technologies (Raman spectrum, Fourier transform infrared spectroscopy (FTIR)) coupled with DFT calculations further disclose that the O-M catalysts prefer the distal association pathway during

the eNRR. These findings can provide a theoretical basis and guidance for exploring the potential of new heterostructure catalysts for the eNRR and other electrochemical fields.

2. RESULTS AND DISCUSSION

Density Functional Theory Calculations. Controllably introducing oxygen into a single Pd metal might be an effective approach to modulate the electron structure of Pd-based catalysts and thus influence their intrinsic eNRR activity and selectivity. Hence, the effect of the oxygen level in Pd/PdO catalysts on their intrinsic electron structure was systematically investigated by DFT calculations. Herein, five atomic models (namely Pd, PdO, O-P, O-M, and O-R Pd/PdO interface) were established as shown in Figures S1–S3 (in the Supporting Information) and Figure 1a–f. The corresponding optimal adsorption energies for N, N₂, and H are summarized in Figures 1g and S4 and Table S1 (in the Supporting Information). The optimal adsorption energies indicated that pure Pd would be unfavorable for N and N₂ adsorption. After the addition of a small amount of oxygen, N₂ was mainly anchored on Pd at the interface of Pd and PdO of the Pd/PdO heterostructures (O-P) and could produce a dramatically increased nitrogen adsorption energy. However, with the increase in the oxygen content, the nitrogen adsorption energy gradually decreased. These results suggested that the introduction of oxygen would efficiently modulate the electronic distribution of pure Pd and nitrogen adsorption ability, thus ultimately affecting the intrinsic eNRR activity of

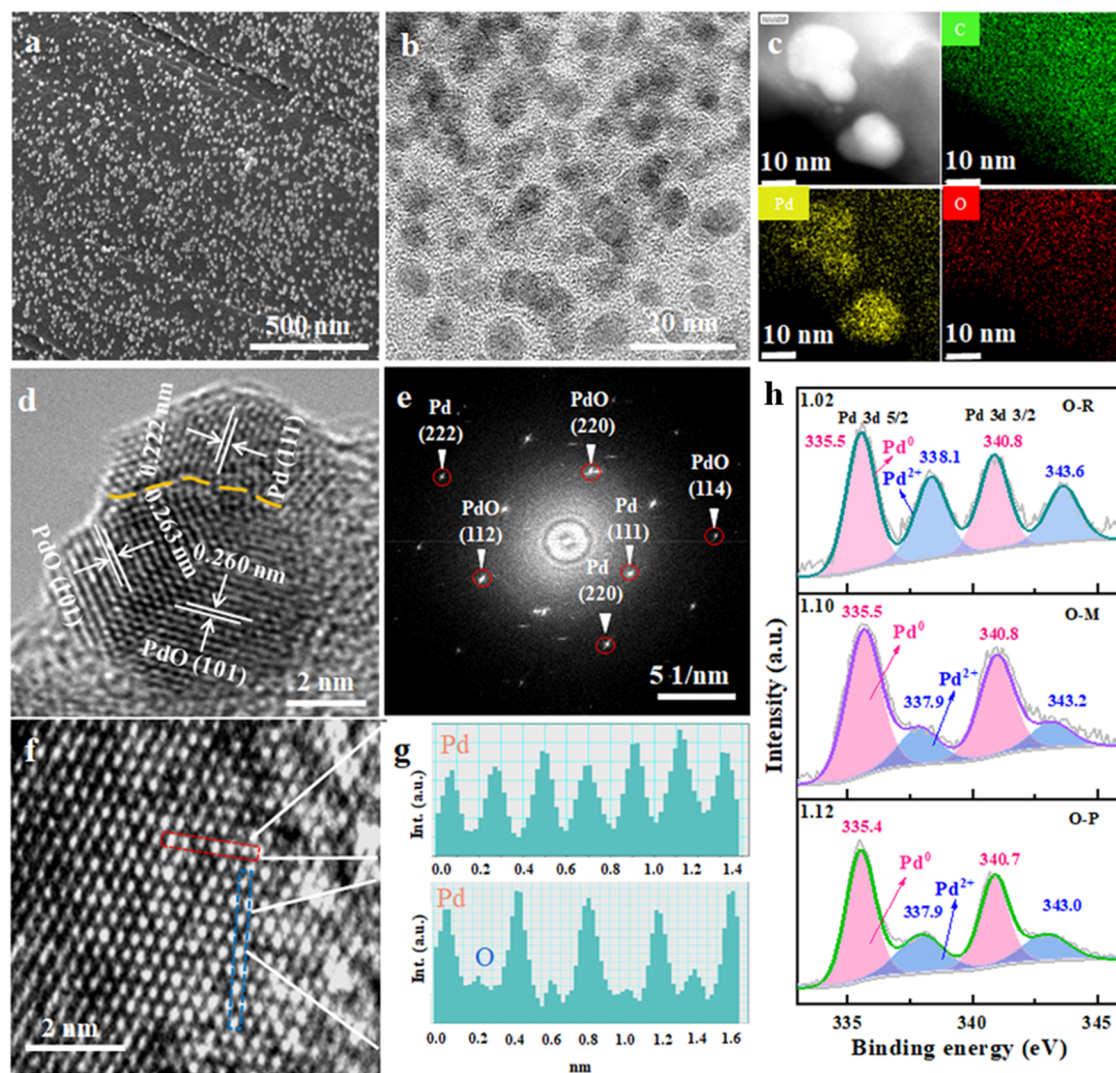


Figure 2. Characterization of the O-M Pd/PdO catalysts. (a) SEM, (b) TEM, (c) the corresponding STEM-EDX elemental mapping, (d) HRTEM, (e) electron diffraction pattern, (f, g) HAADF-STEM images of O-M, and (h) XPS spectra of Pd 3d of three Pd/PdO heterojunction catalysts.

Pd-based catalysts. Similarly, the addition of oxygen also influenced the hydrogen adsorption of the Pd/PdO heterojunctions. A hydrogen atom was anchored on oxygen at the interface of Pd and PdO of the obtained heterojunctions. Compared with pure Pd, the Pd/PdO heterojunctions exhibited higher hydrogen adsorption energies, which indicated that they would intrinsically inhibit the hydrogen evolution reaction (HER) and thus enhance eNRR selectivity. Considering that the electrocatalysts with the moderate adsorption energy for N may facilitate the adsorption and desorption of nitrogen intermediates,^{25,26} we assumed that the O-M Pd/PdO heterojunction may be the most promising eNRR catalyst among the above-mentioned models.

The electron effect of N₂ adsorption on the surface of the catalyst was further investigated by the surface valence band spectrum. From the total density of states (TDOS) in Figure 1h, the conductivity of the system gradually became worse with the increase in the oxygen content, which is consistent with those of the adsorption energy of N₂. The closer the center of the d-band was to the Fermi level (E_f), the adsorbed N₂ was able to form a strong bond with the transition metal surface, thereby promoting electron transfer. The partial density of

state (PDOS in Figure 1i) results indicated that the d-band center (red dotted line) gradually shifted away from E_f in going from O-P to PdO, that is, the adsorption strength of the catalyst to nitrogen gradually weakened. Therefore, the appropriate adsorption strength of the O-M heterojunction catalyst would be the most favorable characteristic for the NRR with the easy activation of N₂ molecules and the efficient desorption of nitrogen intermediates.

Catalyst Design and Structure Identification. Inspired by the exciting computational predictions, facile cyclic voltammetry (CV)-based electrochemical deposited technology was adopted to obtain the O-M Pd/PdO heterojunction electrocatalysts. Herein, an acid-pretreated carbon cloth (CC) was used as the working electrode and preliminarily immersed in an air-filled electrolyte solution containing 25 μ M PdCl₂. For comparison, the control electrocatalysts O-P and O-R Pd/PdO samples were prepared through similar conditions in argon-filled and oxygen-filled electrolytes, respectively (Figure S5 in Supporting Information). As can be seen from the scanning electron microscopy (SEM) and transmission electron microscopy (TEM) images in Figure 2a,b, the obtained O-M electrocatalyst nanoparticles were homoge-

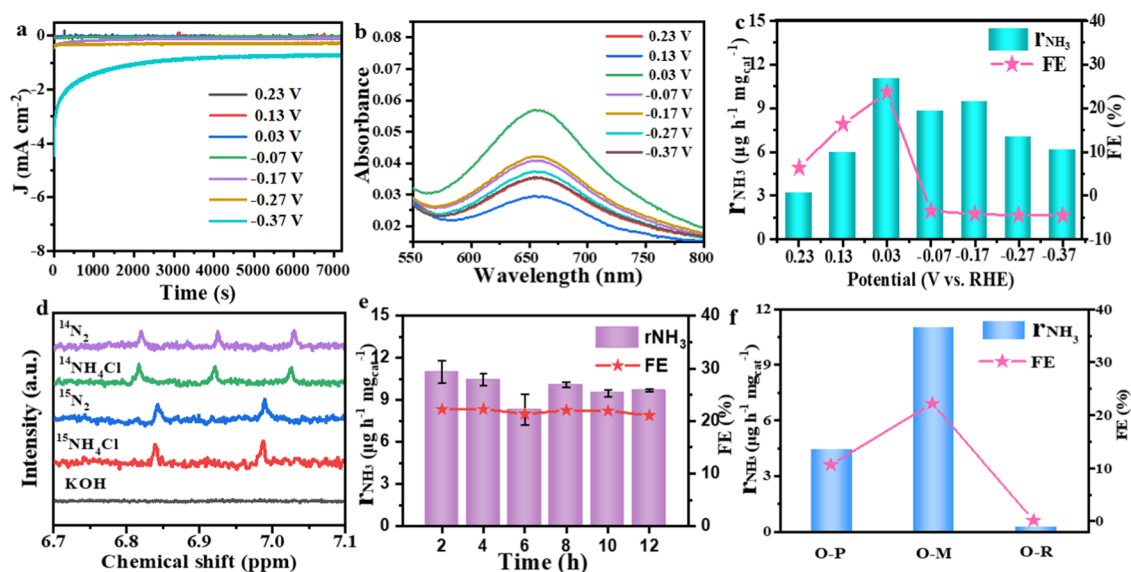


Figure 3. Electrochemical performances of eNRR on the O-M Pd/PdO electrocatalysts. (a) Chronoamperometric curves at different potentials (*vs* RHE) in the N_2 -saturated electrolytes. (b) UV–vis spectra of the electrolytes after electrolysis at different potentials for 2 h. (c) The corresponding NH_3 yield rates (r_{NH_3}) and Faradic efficiencies (FE) at different potentials. (d) 1H NMR spectra (500 MHz) of the standard solution of KOH, $^{15}NH_4^+$, and $^{14}NH_4^+$ and the resultant electrolyte fed with $^{14}N_2$ and $^{15}N_2$. (e) Recycling test. (f) Comparison of the O-M catalyst with the O-P and O-R catalysts for eNRR.

neously dispersed on the CC and their average size was approximately 10 nm. The corresponding scanning TEM energy-dispersive X-ray spectroscopy (STEM-EDX) mappings also showed a homogeneous distribution of the Pd and O elements in the catalyst (Figure 2c). From the high-resolution TEM (HRTEM) image (Figure 2d), two clear interplanar spacings of 0.222 and 0.263 nm were obtained, which corresponded to the planes of Pd (111) and PdO (101), respectively, indicating the presence of a Pd/PdO heterojunction (the yellow dotted line refers to the interface between Pd and PdO). The electron diffraction pattern also clearly revealed different lattice planes of Pd (111), (222), and (220), and faces of PdO (112), (220), and (114) in Pd/PdO (Figure 2e), which indicated that Pd and PdO coexisted in the heterojunction structure. The atomic structure of the O-M Pd/PdO heterojunction was further characterized by high-angle annular dark-field scanning transmission electron microscopy (HAADF-STEM). Figure 2f shows two different atomic structure areas. For area 1 (red area), the bright spots depicted Pd atomic columns (Figure 2g). However, for area 2 (blue area), darker spots were distributed in the brighter atomic columns. The brighter and darker spots were assigned to Pd sites and O sites, respectively, which originate from the higher atomic number of Pd than that of O. These results indicated the coexistence of Pd and PdO in the Pd/PdO heterojunction. The survey XPS spectrum confirmed the presence of C, Pd, and O elements, which further demonstrated that the Pd/PdO catalyst was anchored on CC (Figure S6 in the Supporting Information), in agreement with the elemental mapping results. In the high-resolution Pd 3d spectrum of the O-M catalyst (Figure 2h middle), as observed, there were two pairs of spin–orbit doublets, which indicated the existence of Pd⁰ (binding energy peaks at 335.5 and 340.8 eV) and Pd²⁺ (binding energy peaks at 337.9 and 343.2 eV),^{27–29} further confirming the formation of a Pd/PdO heterojunction. Moreover, with the increase in the oxygen level of the Pd/PdO heterojunctions, the surface content ratio of Pd⁰ to Pd²⁺

gradually decreased through the semiquantitative estimation of the Pd 3d peak area (the value is listed in the upper left corner of Figure 2h). These results provide evidence to support that Pd/PdO catalysts with a tunable oxygen content on CC can be realized by the electrochemical deposition approach.

Catalytic Performance for Nitrogen Reduction Reaction. The eNRR performance of the obtained O-M electrocatalyst was systematically investigated in an H-type electrochemical cell at room temperature and atmospheric pressure. A standard three-electrode system was used in a 0.1 M KOH electrolyte, where the O-M Pd/PdO catalyst on CC was used as the working electrode. All potentials were calibrated with the reversible hydrogen electrode (RHE), unless otherwise noted. To verify if nitrogen contaminant in chemicals or laboratory environment affects the eNRR results, the control experiments were first executed; UV–vis absorption spectra are given in Figure S7. The results exhibit that the positive NRR result is only obtained in an N_2 -saturated electrolyte. Linear scan voltammetry (LSV) was used to preliminarily evaluate the NRR activity of the catalysts. It is obtained from Figure S8 (in the Supporting Information) that the O-M catalyst delivered a higher current density in the N_2 -saturated electrolyte solution than in the Ar-saturated electrolyte solution, which demonstrated that the O-M catalyst is feasible for the eNRR. Figure 3a displays the time-dependent current density curves at constant potentials in an N_2 -saturated electrolyte for 2 h. As the potential became more negative, the current density increased owing to the accelerated eNRR and HER processes. The produced NH_3 in the electrolyte was detected by the indophenol blue colorimetric method³⁰ (the calibration curves as shown in Figure S9 in the Supporting Information) using UV–vis spectroscopy (Figure 3b). Its NH_3 yields and the corresponding FEs under different potentials are plotted in Figure 3c. It was found that the NH_3 yields and FEs gradually increased with the negative potential increase until 0.03 V (*vs* RHE), where it produced an NH_3 yield with $11.0 \mu g h^{-1} mg_{cat}^{-1}$ and a FE with 22.2%. However, with the increase in

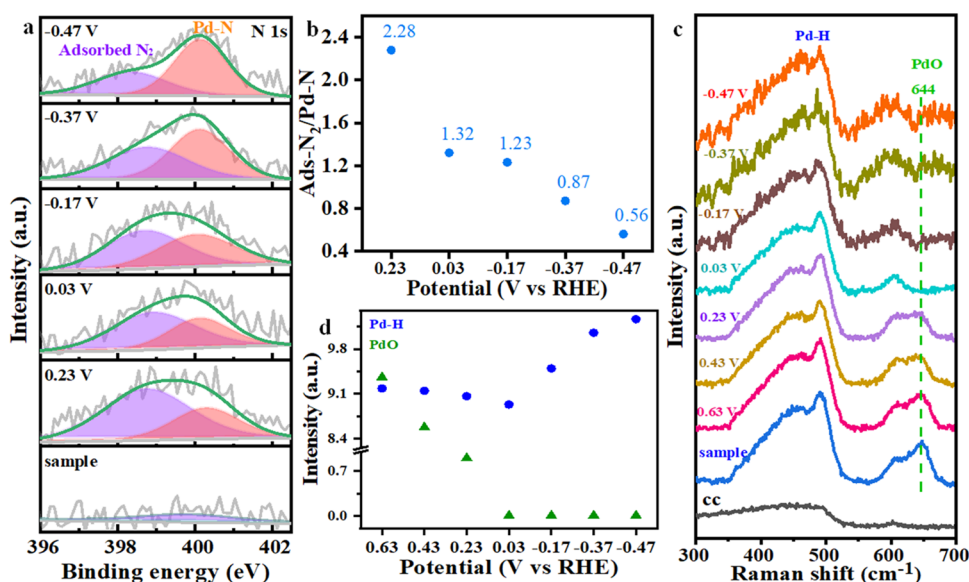


Figure 4. (a) *Ex situ* XPS spectra of N 1s for the O-M Pd/PdO catalysts at different potentials. (b) The corresponding integral intensity area ratio of the adsorbed N₂ to Pd–N (Ads-N₂/Pd–N). (c) *In situ* Raman spectra of the O-M Pd/PdO catalysts for eNRR. (d) Integral intensity of Pd–H and PdO during NRR by *in situ* Raman tests.

negative potential, the NH₃ yields and FEs decreased significantly, which was attributed to the competitive adsorption of nitrogen and hydrogen species on the electrode surface. Furthermore, to clearly identify the origin of the produced NH₃ during eNRR, ¹⁵N₂ isotope labeling experiments were performed on the O-M catalyst. As shown in Figure 3d, dominant peaks of doublet coupling for ¹⁵NH₄⁺ and triplet coupling for ¹⁴NH₄⁺ were seen on the proton nuclear magnetic resonance (¹H NMR) spectra in the case of using ¹⁵N₂ and ¹⁴N₂, respectively, as the feeding gas, which indicated that the N₂ feeding gas was the sole source for the formation of NH₃ from the electrocatalytic NRR. NH₃ was generated exclusively from the electrocatalytic NRR on the electrocatalyst. Additionally, the byproduct hydrazine (N₂H₄) was not detected in the O-M Pd/PdO-based electrocatalyst system by the Watt and Chrisp method³¹ (Figures S9 and S10 in the Supporting Information). In terms of recycling stability, several consecutive constant potential electrolysis runs were carried out at 0.03 V (*vs* RHE). As can be seen from Figure 3e, there were negligible changes in the NH₃ yields and the corresponding FEs. Furthermore, the corresponding structure and morphology of the O-M Pd/PdO catalysts still exhibited no change through TEM (Figure S11 in the Supporting Information), which indicated high stability of the O-M Pd/PdO-based electrocatalyst system. In addition, the control catalysts O-P and O-R heterojunctions for eNRR were systematically investigated in the same conditions. As can be seen from Figure 3f, the NH₃ yield and FEs of the O-M catalyst were obviously higher than those of the O-P and O-R catalysts. The sharp decrease in the catalytic activity of Pd/PdO (O-R) is mainly ascribed to the relatively poor conductivity, the weakened adsorption strength to nitrogen, and the rapid rising of the HER activity, consistent with the theoretical calculation results. Furthermore, the O-M catalyst for the eNRR under optimal conditions produced a comparable electrocatalytic performance to those of the reported electrocatalysts (Table S2 in the Supporting Information). These results demonstrated that the Pd/PdO

heterojunction could boost their intrinsic eNRR activity and selectivity *via* controllably modulating the oxygen level.

Ex Situ XPS and In Situ Raman Spectroscopy Measurements. To verify the surface conversion of the O-M Pd/PdO heterojunction catalyst, *ex situ* XPS was applied. As shown in the high-resolution Pd 3d spectrum in Figures S12 and S13 (in the Supporting Information), the intensity ratio of Pd⁰ to Pd²⁺ gradually increased during the eNRR process owing to the reduction of more Pd²⁺ to Pd⁰ under a more negative potential. Furthermore, as given in Figure 4a, before N₂ reduction, no N signal was observed in the high-resolution XPS spectrum of N 1s. During the eNRR process, two peaks appeared at binding energies (BEs) of ~398 and ~400 eV in the N 1s spectrum, which corresponded to the adsorbed N₂ and Pd–N, respectively.³² Notably, the intensity ratio of the adsorbed N₂ (Ads-N₂) to Pd–N was obviously decreased during the NRR process with the decrease in the applied potential (Figure 4b), which indicated that Ads-N₂ may transfer to the Pd–N bond in the heterojunction structure of Pd/PdO, thus enhancing the NRR performance. To further understand the possible reaction mechanism of the O-M catalyst, *in situ* Raman spectroscopy was applied under various potentials.^{33,34} As given in Figure 4c, two new peaks appearing at 487 and 644 cm⁻¹ were assigned to the Pd–H band and the PdO band,^{35–37} respectively, compared with those of the blank carbon cloth substrate (Figure S14 in the Supporting Information). The corresponding peaks intensities during the eNRR process for the O-M catalyst are shown in Figure 4d. As the potential shifted from 0.63 to 0.03 V, the intensity of PdO dropped, which indicated that PdO was dramatically reduced and Pd tended to preferentially adsorb N atoms, in agreement with *ex situ* XPS results. Meanwhile, the intensity of Pd–H was slightly decreased, which resulted in the suppression of the competition reaction of HER. In contrast, as the potential became more negative (from 0.03 to –0.47 V), the intensity of Pd–H sharply increased owing to the stronger HER performance, thus lowering the NH₃ yield and FEs (Figure 3c). Therefore, the O-M catalysts exhibited the highest NH₃ yield and good selectivity at 0.03 V (Figure 3c), which could

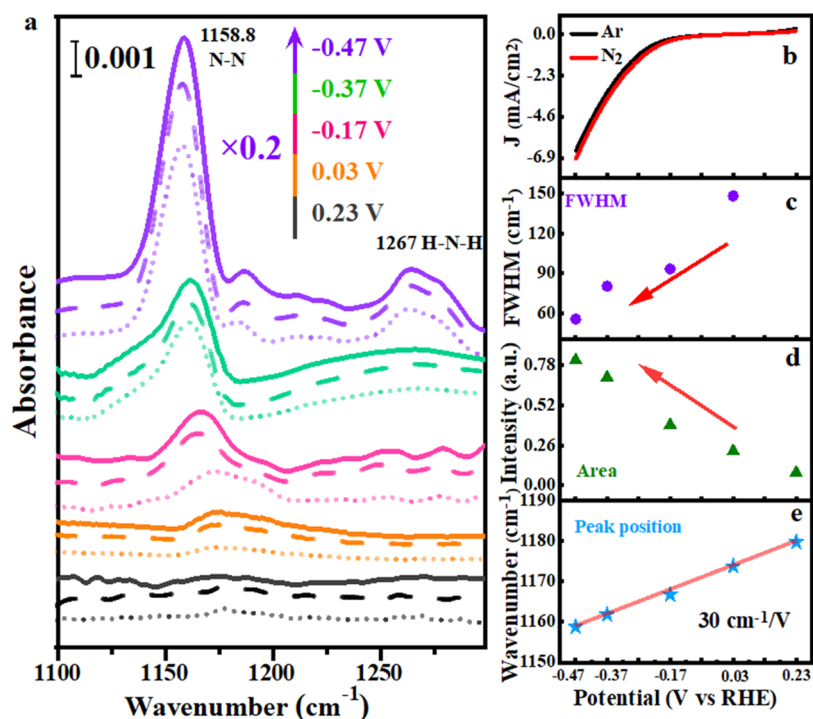


Figure 5. (a) *In situ* FTIR spectra of the O-M catalysts at different potentials. (b) LSV curves of O-M catalyst for eNRR in N_2 -saturated and Ar-saturated electrolyte solutions, respectively. The potential dependence of (c) FWHM, (d) integral area of the peak intensity, and (e) peak position of N–N bending during the eNRR process catalyzed by the O-M catalysts.

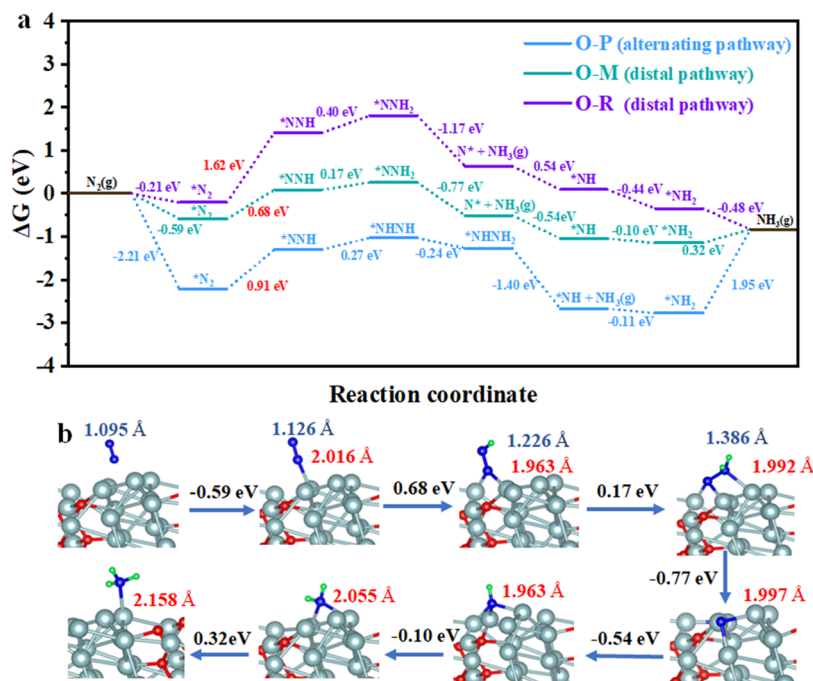


Figure 6. (a) Energy diagrams of eNRR on the O-P, O-M, and O-R catalysts. (b) Schematic diagram of the possible distal pathways of the O-M catalysts for the eNRR and the corresponding bond lengths of N–N (blue) and Pd–N (red). The Pd, N, O, and H atoms are presented by silvery gray, blue, red, and green solid balls, respectively.

be attributed to the fact that the moderate affinity of Pd to N in the Pd/PdO heterojunction and the inhibition of HER could facilitate the breaking of the triple bond of N_2 and promote the protonation of N and accelerate the NRR process.

***In Situ* Fourier Transform Infrared Spectroscopy Measurements.** To further investigate the produced nitrogen

intermediates catalyzed by the O-M catalyst during the eNRR process within the potential from 0.23 to -0.47 V, *in situ* Fourier transform infrared spectroscopy (FTIR) measurements were carried out, as shown in Figure 5a.^{38,39} The spectrum corresponding to the initial 0.23 V, where no reaction occurred (Figure 5b), was regarded as a reference, and the spectral

variations at subsequent potentials were attributed to the electrochemical reaction induced by the potential change. Under the treatment of constant potential at -0.47 V, the obvious bands at 1267 and 1158 cm^{-1} were observed and assigned to the H–N–H bending vibration and N–N stretching vibration, respectively. Combined with the LSV curves in Figure 5b, it can be seen that these results indicated the breakage of the N \equiv N triple bonds and the production of nitrogen intermediates on the electrode surface. To better illustrate the spectroscopic variations within the cathode material during the eNRR process, the potential dependence of the full width at half-maximum (FWHM), the integral area of the peak intensity, and the peak position of N–N bending are given in Figure 5c–e, respectively. The peak position of the N–N bond was shifted at a rate of 30 cm^{-1}/V , which is attributed to the Stark effect.^{40,41} The band intensity of N–N bending was enhanced with the increase in the applied potential. Meanwhile, their FWHM gradually decreased and the band become sharp, which suggested that N₂ molecules were continuously activated and reduced on the surface of the heterojunction. Furthermore, the absence of detectable hydrazine peaks confirmed the high selectivity of the O–M catalysts for the eNRR. We might deduce that the O–M catalyst possibly underwent the distal association pathway to a lower N₂ activation barrier and promote NRR kinetics.

Pathway for NRR by DFT Calculations. Density functional theory (DFT) calculations were carried out to understand the energetic NRR pathway for the produced Pd/PdO heterojunction catalysts.^{42,43} The Gibbs free energy diagrams of the electrochemical reduction of N₂ to NH₃ on the surface of the optimized heterojunction catalysts are displayed in Figures 6a and S15–S17 (in the Supporting Information). It can be seen that the potential-determining steps (PDS) are $^*\text{NH}_2 \rightarrow \text{NH}_3$ (g), $^*\text{N}_2 \rightarrow ^*\text{NNH}$, and $^*\text{N}_2 \rightarrow ^*\text{NNH}$ for the O–P, O–M, and O–R catalysts, respectively, which indicated that the O–M and O–R catalysts followed the distal pathway and the O–P catalyst abided by the alternative pathway. Meanwhile, it can be clearly seen from Figure 6a that the O–M catalyst exhibits a lower Gibbs free energy compared with those of the O–P and O–R catalysts, indicating that it is most suitable for eNRR. Furthermore, the N₂ molecules transformed into the adsorption species on the surface of the O–M catalyst during the reaction process, and the N–N bond length (blue) changed from 1.095 to 1.126 Å (Figure 6b), which indicated that the N₂ molecules were activated on the surface of the catalyst. Meanwhile, the N–N bond length in the process of $^*\text{NNH} \rightarrow ^*\text{NNH}_2$ increased from 1.226 to 1.386 Å, which facilitated the stripping of NH₃ (g). Additionally, the Pd–N bond length (gray) increased from 1.997 to 2.158 Å during the second generation of NH₃ (g), which also showed that the product was an efficient desorption process. Therefore, by combining the *ex situ* XPS, *in situ* Raman, and *in situ* FTIR results, we further confirmed that the high performance of eNRR on the optimal O–M catalyst originated from the important energetic preference of N₂ fixation and efficient hydrogenation during the NRR process.

3. CONCLUSIONS

In summary, we successfully prepared the Pd/PdO heterojunction with controllable oxygen content through the electrochemical deposition approach at different gas atmospheres. The O–M Pd/PdO heterojunction reached the NH₃ yield of 11.0 $\mu\text{g h}^{-1} \text{mg}_{\text{cat}}^{-1}$ and a large FE of 22.2% at 0.03 V

versus RHE in 0.1 M KOH electrolyte, accompanied by good stability under alkaline conditions. These can be attributed to the moderate affinity of Pd to N in the Pd/PdO heterojunction and the inhibition of HER to facilitate the breaking of the triple bond of N₂ and promote the protonation of N, confirmed by *in situ* Raman and *ex situ* XPS. The eNRR on the surface of the O–M Pd/PdO heterojunction prefers to occur along the distal association pathway, observed from *in situ* FTIR and DFT calculations. Therefore, this work can encourage and guide further research on the development of other heterojunction catalysts for renewable energy applications.

■ ASSOCIATED CONTENT

Supporting Information

The Supporting Information is available free of charge at <https://pubs.acs.org/doi/10.1021/acsami.2c02329>.

Experimental sections, adsorption sites and adsorption energies of N, N₂, and H on different models (Pd, PdO, O–P, O–M, O–R), Gibbs free energy of HER over Pd, PdO, O–P, O–M, and O–R models, SEM, TEM, and SEDA patterns for O–P, O–M, and O–R, XPS survey spectrum of the O–M catalysts, LSV curves of the O–M catalyst for eNRR in the N₂-saturated and Ar-saturated electrolyte solutions, UV–vis absorption spectra of the ammonia and hydrazine standard solutions and the corresponding calibration curves, UV–vis spectra of the byproduct hydrazine in the electrolytes after eNRR, SEM images of O–P, O–M, and O–R after NRR tests, *ex situ* XPS spectra of Pd 3d for the O–M Pd/PdO heterojunction catalyst during eNRR at different potentials, the corresponding integral intensity area ratio of Pd⁰ to Pd²⁺ (Pd(0)/Pd(II)) for O–M catalyst during the eNRR process, *in situ* Raman spectra of bare carbon cloth for eNRR, and Gibbs free energy and reaction pathway of the Pd/PdO heterojunctions (O–P, O–M, O–R) for eNRR are presented (PDF)

■ AUTHOR INFORMATION

Corresponding Authors

Xuemei Zhou – Key Laboratory of Carbon Materials of Zhejiang Province, College of Chemistry and Materials Engineering, Wenzhou University, Wenzhou 325035, China; Email: zxm.mei@163.com

Huagui Nie – Key Laboratory of Carbon Materials of Zhejiang Province, College of Chemistry and Materials Engineering, Wenzhou University, Wenzhou 325035, China; Email: huaguinie@126.com

Zhi Yang – Key Laboratory of Carbon Materials of Zhejiang Province, College of Chemistry and Materials Engineering, Wenzhou University, Wenzhou 325035, China; orcid.org/0000-0002-9265-5041; Email: yang201079@126.com

Authors

Qianqian Chen – Key Laboratory of Carbon Materials of Zhejiang Province, College of Chemistry and Materials Engineering, Wenzhou University, Wenzhou 325035, China
Xiaodong Zhang – Key Laboratory of Carbon Materials of Zhejiang Province, College of Chemistry and Materials Engineering, Wenzhou University, Wenzhou 325035, China

Wenjie Luo – Key Laboratory of Carbon Materials of Zhejiang Province, College of Chemistry and Materials Engineering, Wenzhou University, Wenzhou 325035, China

Shuo Yang – College of Electrical and Electronic Engineering, Wenzhou University, Wenzhou 325035, China;

orcid.org/0000-0001-8906-5289

Yongjie Ge – Key Laboratory of Carbon Materials of Zhejiang Province, College of Chemistry and Materials Engineering, Wenzhou University, Wenzhou 325035, China

Dong Cai – Key Laboratory of Carbon Materials of Zhejiang Province, College of Chemistry and Materials Engineering, Wenzhou University, Wenzhou 325035, China

Complete contact information is available at:

<https://pubs.acs.org/10.1021/acsami.2c02329>

Author Contributions

The manuscript was written through contributions of all authors. All authors have given approval to the final version of the manuscript.

Notes

The authors declare no competing financial interest.

ACKNOWLEDGMENTS

This work was supported in part by the National Natural Science Foundation of China (Grant Nos. 22109119, 51972238, 22105147, and 21875166), the Natural Science Foundation of Zhejiang Province (Grant Nos. LR18E020001 and LQ22B030003), the Basic Scientific Research Projects of Wenzhou City (Grant Nos. G2020002 and H20210006), and Major Scientific and Technological Innovation Project of Wenzhou City (Grant No. ZG2021013).

REFERENCES

- (1) Qing, G.; Ghazfar, R.; Jackowski, S. T.; Habibzadeh, F.; Ashtiani, M. M.; Chen, C. P.; Smith, M. R., 3rd; Hamann, T. W. Recent Advances and Challenges of Electrocatalytic N₂ Reduction to Ammonia. *Chem. Rev.*, **2020**, *120*, 5437–5516.
- (2) Tang, C.; Qiao, S. Z. How to explore ambient electrocatalytic nitrogen reduction reliably and insightfully. *Chem. Soc. Rev.*, **2019**, *48*, 3166–3180.
- (3) Zhao, R.; Xie, H.; Chang, L.; Zhang, X.; Zhu, X.; Tong, X.; Wang, T.; Luo, Y.; Wei, P.; Wang, Z.; Sun, X. Recent progress in the electrochemical ammonia synthesis under ambient conditions. *J. Energy Chem.* **2019**, *1*, No. 100011.
- (4) Cui, X.; Tang, C.; Zhang, Q. A Review of Electrocatalytic Reduction of Dinitrogen to Ammonia under Ambient Conditions. *Adv. Energy Mater.* **2018**, *8*, No. 1800369.
- (5) Légaré, M.-A.; Bélanger-Chabot, G.; Dewhurst, R. D.; Welz, E.; Krummenacher, I.; Engels, B.; Braunschweig, H. Nitrogen fixation and reduction at boron. *Science* **2018**, *359*, 896–900.
- (6) Chen, G. F.; Ren, S.; Zhang, L.; Cheng, H.; Luo, Y.; Zhu, K.; Ding, L. X.; Wang, H. Advances in Electrocatalytic N₂ Reduction—Strategies to Tackle the Selectivity Challenge. *Small Methods* **2018**, *3*, No. 1800337.
- (7) Chen, Q.; Zhang, X.; Jin, Y.; Zhou, X.; Yang, Z.; Nie, H., An Overview on Noble Metal (Group VIII)-based Heterogeneous Electrocatalysts for Nitrogen Reduction Reaction. *2020*, *15*, 4131–4152.
- (8) Andersen, S. Z.; Colic, V.; Yang, S.; Schwalbe, J. A.; Nielander, A. C.; McEnaney, J. M.; Enemark-Rasmussen, K.; Baker, J. G.; Singh, A. R.; Rohr, B. A.; Statt, M. J.; Blair, S. J.; Mezzavilla, S.; Kibsgaard, J.; Vesborg, P. C. K.; Cargnello, M.; Bent, S. F.; Jaramillo, T. F.; Stephens, I. E. L.; Nørskov, J. K.; Chorkendorff, I. A rigorous electrochemical ammonia synthesis protocol with quantitative isotope measurements. *Nature* **2019**, *570*, 504–508.
- (9) Li, S.; Luo, Y.; Yue, L.; Li, T.; Wang, Y.; Liu, Q.; Cui, G.; Zhang, F.; Asiri, A. M.; Sun, X. An amorphous WC thin film enabled high-efficiency N₂ reduction electrocatalysis under ambient conditions. *Chem. Commun.* **2021**, *57*, 7806–7809.
- (10) Li, S.; Wu, Y.; Liu, Q.; Li, B.; Li, T.; Zhao, H.; Alshehri, A. A.; Alzahrani, K. A.; Luo, Y.; Li, L.; Sun, X. CuS concave polyhedral superstructures enabled efficient N₂ electroreduction to NH₃ at ambient conditions. *Inorg. Chem. Front.* **2021**, *8*, 3105–3110.
- (11) Chen, G.-F.; Cao, X.; Wu, S.; Zeng, X.; Ding, L.-X.; Zhu, M.; Wang, H. Ammonia electrosynthesis with high selectivity under ambient conditions via a Li⁺ incorporation strategy. *J. Am. Chem. Soc.* **2017**, *139*, 9771–9774.
- (12) Kani, N. C.; Prajapati, A.; Collins, B. A.; Goodpaster, J. D.; Singh, M. R. Competing Effects of pH, Cation Identity, H₂O Saturation, and N₂ Concentration on the Activity and Selectivity of Electrochemical Reduction of N₂ to NH₃ on Electrodeposited Cu at Ambient Conditions. *ACS Catal.* **2020**, *10*, 14592–14603.
- (13) Hao, Y.-C.; Guo, Y.; Chen, L.-W.; Shu, M.; Wang, X.-Y.; Bu, T.-A.; Gao, W.-Y.; Zhang, N.; Su, X.; Feng, X.; et al. Promoting nitrogen electroreduction to ammonia with bismuth nanocrystals and potassium cations in water. *Nat. Catal.* **2019**, *2*, 448–456.
- (14) Liu, H.-M.; Han, S.-H.; Zhao, Y.; Zhu, Y.-Y.; Tian, X.-L.; Zeng, J.-H.; Jiang, J.-X.; Xia, B. Y.; Chen, Y. Surfactant-free atomically ultrathin rhodium nanosheet nanoassemblies for efficient nitrogen electroreduction. *J. Mater. Chem. A* **2018**, *6*, 3211–3217.
- (15) Xu, T.; Liang, J.; Wang, Y.; Li, S.; Du, Z.; Li, T.; Liu, Q.; Luo, Y.; Zhang, F.; Shi, X.; Tang, B.; Kong, Q.; Asiri, A. M.; Yang, C.; Ma, D.; Sun, X. Enhancing electrocatalytic N₂-to-NH₃ fixation by suppressing hydrogen evolution with alkythiols modified Fe₃P nanoarrays. *Nano Res.* **2022**, *15*, 1039–1046.
- (16) Wang, J.; Yu, L.; Hu, L.; Chen, G.; Xin, H.; Feng, X. Ambient ammonia synthesis via palladium-catalyzed electrohydrogenation of dinitrogen at low overpotential. *Nat. Commun.* **2018**, *9*, No. 1795.
- (17) Deng, G.; Wang, T.; Alshehri, A. A.; Alzahrani, K. A.; Wang, Y.; Ye, H.; Luo, Y.; Sun, X. Improving the electrocatalytic N₂ reduction activity of Pd nanoparticles through surface modification. *J. Mater. Chem. A* **2019**, *7*, 21674–21677.
- (18) Qian, Y.; Liu, Y.; Zhao, Y.; Zhang, X.; Yu, G. Single vs double atom catalyst for N₂ activation in nitrogen reduction reaction: A DFT perspective. *EcoMat* **2020**, *2*, No. e12014.
- (19) Chen, H.; Liang, J.; Li, L.; Zheng, B.; Feng, Z.; Xu, Z.; Luo, Y.; Liu, Q.; Shi, X.; Liu, Y.; Gao, S.; Asiri, A. M.; Wang, Y.; Kong, Q.; Sun, X. Ti₂O₃ Nanoparticles with Ti³⁺ Sites toward Efficient NH₃ Electrosynthesis under Ambient Conditions. *ACS Appl. Mater. Interfaces* **2021**, *13*, 41715–41722.
- (20) Chen, H.; Liang, J.; Dong, K.; Yue, L.; Li, T.; Luo, Y.; Feng, Z.; Li, N.; Hamdy, M. S.; Alshehri, A. A.; Wang, Y.; Sun, X.; Liu, Q. Ambient electrochemical N₂-to-NH₃ conversion catalyzed by TiO₂ decorated juncus effusus-derived carbon microtubes. *Inorg. Chem. Front.* **2022**, *9*, 1514–1519.
- (21) Wang, Z.; Li, C.; Deng, K.; Xu, Y.; Xue, H.; Li, X.; Wang, L.; Wang, H. Ambient nitrogen reduction to ammonia electrocatalyzed by bimetallic PdRu porous nanostructures. *ACS Sustainable Chem. Eng.* **2019**, *7*, 2400–2405.
- (22) Lv, J.; Wu, S.; Tian, Z.; Ye, Y.; Liu, J.; Liang, C. Construction of PdO–Pd interfaces assisted by laser irradiation for enhanced electrocatalytic N₂ reduction reaction. *J. Mater. Chem. A* **2019**, *7*, 12627–12634.
- (23) Yang, L.; Shaik, F.; Pang, F.; Zhang, W. PdAgCu Alloy Nanoparticles Integrated on Three-Dimensional Nanoporous CuO for Efficient Electrocatalytic Nitrogen Reduction under Ambient Conditions. *Langmuir* **2020**, *36*, 5112–5117.
- (24) Zhou, J.; Liu, X.; Xu, X.; Sun, X.; Wu, D.; Ma, H.; Ren, X.; Wei, Q.; Ju, H. Interface Engineering of CoS₂–CeO₂/Ti Nanocatalyst for Artificial N₂ Fixation. *ACS Sustainable Chem. Eng.* **2021**, *9*, 13399–13405.
- (25) Liu, X.; Jiao, Y.; Zheng, Y.; Jaroniec, M.; Qiao, S.-Z. Building up a picture of the electrocatalytic nitrogen reduction activity of

transition metal single-atom catalysts. *J. Am. Chem. Soc.* **2019**, *141*, 9664–9672.

(26) Skúlason, E.; Bligaard, T.; Gudmundsdóttir, S.; Studt, F.; Rossmeisl, J.; Abild-Pedersen, F.; Vegge, T.; Jonsson, H.; Nørskov, J. K. A theoretical evaluation of possible transition metal electrocatalysts for N₂ reduction. *Phys. Chem. Chem. Phys.* **2012**, *14*, 1235–1245.

(27) Hoflund, G. B.; Hagelin, H. A. E.; Weaver, J. F.; Salaita, G. N. ELS and XPS study of Pd/PdO methane oxidation catalysts. *Appl. Surf. Sci.* **2003**, *205*, 102–112.

(28) Lv, Q.; Meng, Q.; Liu, W.; Sun, N.; Jiang, K.; Ma, L.; Peng, Z.; Cai, W.; Liu, C.; Ge, J.; Liu, L.; Xing, W. Pd–PdO Interface as Active Site for HCOOH Selective Dehydrogenation at Ambient Condition. *J. Phys. Chem. C* **2018**, *122*, 2081–2088.

(29) Zhang, P.; Gong, Y.; Li, H.; Chen, Z.; Wang, Y. Solvent-free aerobic oxidation of hydrocarbons and alcohols with Pd@N-doped carbon from glucose. *Nat. Commun.* **2013**, *4*, No. 1593.

(30) Kim, H. S.; Choi, J.; Kong, J.; Kim, H.; Yoo, S. J.; Park, H. S. Regenerative Electrocatalytic Redox Cycle of Copper Sulfide for Sustainable NH₃ Production under Ambient Conditions. *ACS Catal.* **2021**, *11*, 435–445.

(31) Yu, H.; Wang, Z.; Yin, S.; Li, C.; Xu, Y.; Li, X.; Wang, L.; Wang, H. Mesoporous Au₃Pd Film on Ni Foam: A Self-Supported Electrocatalyst for Efficient Synthesis of Ammonia. *ACS Appl. Mater. Interfaces* **2020**, *12*, 436–442.

(32) Zhan, Y.; Zhou, X.; Nie, H.; Xu, X.; Zheng, X.; Hou, J.; Duan, H.; Huang, S.; Yang, Z. Designing Pd/O co-doped MoS_x for boosting the hydrogen evolution reaction. *J. Mater. Chem. A* **2019**, *7*, 15599–15606.

(33) Zhou, S.; Yang, S.; Ding, X.; Lai, Y.; Nie, H.; Zhang, Y.; Chan, D.; Duan, H.; Huang, S.; Yang, Z. Dual-Regulation Strategy to Improve Anchoring and Conversion of Polysulfides in Lithium–Sulfur Batteries. *ACS Nano* **2020**, *14*, 7538–7551.

(34) Zhong, H.; Wang, M.; Ghorbani-Asl, M.; Zhang, J.; Ly, K. H.; Liao, Z.; Chen, G.; Wei, Y.; Biswal, B. P.; Zschech, E.; Weidinger, I. M.; Krashennnikov, A. V.; Dong, R.; Feng, X. Boosting the Electrocatalytic Conversion of Nitrogen to Ammonia on Metal-Phthalocyanine-Based Two-Dimensional Conjugated Covalent Organic Frameworks. *J. Am. Chem. Soc.* **2021**, *143*, 19992–20000.

(35) Sherman, R.; Birnbaum, H. K.; Holy, J. A.; Klein, M. V. Raman studies of hydrogen vibrational modes in palladium. *Phys. Lett. A* **1977**, *62*, 353–355.

(36) Bardhan, R.; Zarick, H. F.; Schwartzberg, A.; Pint, C. L. Size-Dependent Phononic Properties of PdO Nanocrystals Probed by Nanoscale Optical Thermometry. *J. Phys. Chem. C* **2013**, *117*, 21558–21568.

(37) Zhao, Z.; Elwood, J.; Carpenter, M. A. Phonon Anharmonicity of PdO Studied by Raman Spectrometry. *J. Phys. Chem. C* **2015**, *119*, 23094–23102.

(38) Yao, Y.; Zhu, S.; Wang, H.; Li, H.; Shao, M. A Spectroscopic Study on the Nitrogen Electrochemical Reduction Reaction on Gold and Platinum Surfaces. *J. Am. Chem. Soc.* **2018**, *140*, 1496–1501.

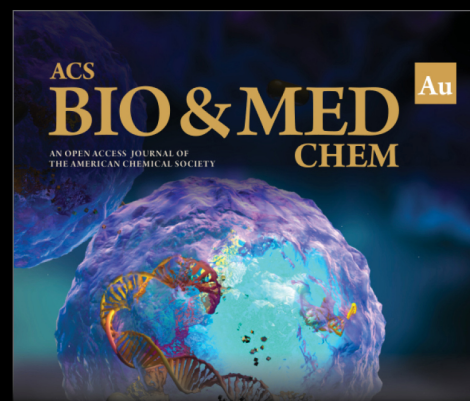
(39) Yao, Y.; Wang, H.; Yuan, X.-z.; Li, H.; Shao, M. Electrochemical Nitrogen Reduction Reaction on Ruthenium. *ACS Energy Lett.* **2019**, *4*, 1336–1341.

(40) Ma, M.; Yan; Wang, J.-Y.; Li, Q.-X.; Cai, W.-B. A Study of NO Adducts of Iron Protoporphyrin IX Adlayer on Au Electrode with in Situ ATR-FTIR Spectroscopy. *J. Phys. Chem. C* **2007**, *111*, 8649–8654.

(41) Molina Concha, B.; Chatenet, M.; Ticianelli, E. A.; Lima, F. H. B. In Situ Infrared (FTIR) Study of the Mechanism of the Borohydride Oxidation Reaction on Smooth Pt Electrode. *J. Phys. Chem. C* **2011**, *115*, 12439–12447.

(42) Tanaka, H.; Mori, H.; Seino, H.; Hidai, M.; Mizobe, Y.; Yoshizawa, K. DFT Study on Chemical N₂ Fixation by Using a Cubane-Type RuIr₃S₄ Cluster: Energy Profile for Binding and Reduction of N₂ to Ammonia via Ru–N–NH_x (x = 1–3) Intermediates with Unique Structures. *J. Am. Chem. Soc.* **2008**, *130*, 9037–9047.

(43) Liu, P.; Fu, C.; Li, Y.; Wei, H. Theoretical screening of single atoms anchored on defective graphene for electrocatalytic N₂ reduction reactions: a DFT study. *Phys. Chem. Chem. Phys.* **2020**, *22*, 9322–9329.



Editor-in-Chief: **Prof. Shelley D. Minteer**, University of Utah, USA



Deputy Editor
Prof. Squire J. Booker
Pennsylvania State University, USA

Open for Submissions 

pubs.acs.org/biomedchemau

 **ACS Publications**
Most Trusted. Most Cited. Most Read.